Abstract

In vertebrates, macrophages are critical innate immune cells of which a specialized subset called microglia resides in the brain integrated with neurons and other glial cells. While microglia have been implicated for many functions in the brain, it has remained unclear whether these immune cells can influence animal behaviors though modulating brain neural circuits. We hypothesized that microglia are intricately interconnected with neuronal activity and thus neural circuit function, thereby able to alter behavioral outputs of brain functions. We sought to use genetic models, namely the microglia-lacking zebrafish *nlrc3l* and *irf8* mutants, to understand whether eliminating the normal interactions of microglia in the brain could lead to altered behaviors. We performed large-scale, long-term movement tracking and found a highly significant reduction in spontaneous locomotion during daytime in the *nlrc3l* mutants, while the other microglia-lacking mutant (*irf8* mutant) exhibited only a modest difference. We also analyzed the pattern of movement over the long-term tracking, and found no significant difference between the mutants from control animals, indicating the phenotype was specific to a decrease in spontaneous activity rather than a defect in pattern of movement or ability to move. Using *in vivo* whole-brain calcium imaging, we found a strong reduction in baseline neural firing in the diencephalic neurons of the *nlrc3l* mutants. Further analysis of additional brain regions and other microglia-lacking mutants will better define specific neural circuits susceptible to microglial regulation, thereby altered in the absence of microglia. This study provides evidence supporting the role of microglia in modulating neural circuits that regulate normal spontaneous behaviors at steady state and the possibility that the presence of inflammation can exacerbate the behavioral deficiency when microglia are impaired. Insights from our zebrafish paradigm can shed light on neuroimmune interactions that likely will be relevant to these

processes in human as many genetic pathways and cellular mechanisms are conserved between zebrafish and human.

Introduction

Macrophages play a critical role in mediating immune responses to foreign stimuli and clearing damaging particles or dying cells to protect the host. Microglia are brain-resident macrophages important for clearing away neuronal corpses during apoptosis in the developing brain in vertebrates. While many studies focus on understanding the underlying neural mechanisms controlling various types of stimulated animal behaviors, much less is known about how the immune system may cross-regulate the nervous system by controlling neural circuit functions impacting behavioral outputs.

Previous genetics studies have revealed genes critical for the identity, development and function of macrophages and microglia in zebrafish. For example, mfap4 and mpeg1 are known macrophage markers in zebrafish (1–4). Several previous studies of my research advisor have uncovered new genetic zebrafish mutants that have a complete elimination of microglia during development. One of these studies showed that a zebrafish ortholog of the phosphate receptor xpr1, *xpr1b* is shown to be required for the tissue-specific differentiations of primitive macrophages in zebrafish (5). Another as reported in Shiau et al.(6), they identified an anti-inflammatory nod-like receptor *nrlc3l* that is required for microglia development, because knockout of nlrc3l surprisingly causes unwarranted auto-activation of macrophages that triggers systemic inflammation in the nlrc3l mutants. A third study showed that a member of the interferon regulatory factor (IRF) family, *irf8* is critical in the early specification of macrophages in zebrafish, whereby *irf8* null mutants do not have microglia or *mfap4*-expressing macrophages, but later some macrophages recover in adults (7).

Given the critical role of microglia during the neuronal apoptosis, the early disruption of microglia may have long-term consequences on brain development and function. Moreover, the function of microglia has been shown to be more than removal of neuronal apoptoses. Cell culture studies have shown that microglia express receptors for neurotransmitters such as GABA, glutamate and dopamine (8); microglia can contact neurons physically and is also capable of synaptic stripping (9). Additionally, Li et al. (10) has reported the reciprocal relationship between neurons with activated pannexin-1 hemichannels and in the optic tectum of larval zebrafish and resting microglial processes *in vivo*; their study suggests the potential role of microglia in the regulation of neuronal activities in the healthy brain at homeostasis. Given these previous studies, microglia might actively modulate the neuronal activity in the brain, thereby contributing to the formation and maintenance of the brain neural circuits.

We hypothesized that microglia are intricately interconnected with neuronal activity and thus neural circuit function, thereby able to alter behavioral outputs of brain functions. As a starting point to test this idea, we sought to use genetic models, namely zebrafish *nlrc3l* and *irf8* mutants, which lack microglia to understand whether eliminating the normal interactions of microglia in the brain could lead to altered normal zebrafish behaviors. These mutant animals are morphologically normal and indistinguishable from wild type, and therefore any behavioral changes will likely be attributed to an altered brain function. We conducted large-scale, high-throughput parallel locomotion tracking of these mutants compared with their control wild type and heterozygous siblings in a neutral, stimulus-free environment. To investigate possible neuronal activity change due to microglial loss, we leveraged whole brain *in vivo* GCaMP6f imaging, by capturing fluctuations of neuronal cytoplasmic calcium ion (Ca^{2+}) concentrations as a proxy for neuronal firings. To examine molecular pathways that may be disrupted in the microglia-

lacking *nlrc3l* mutants in causing the striking behavioral deficiency, we employed a genome-wide transcriptome analysis by RNA-sequencing (RNA-Seq).

The goal of this study was to determine whether microglia have a role in regulating steady state normal brain neural activity that controlled animal behaviors at homeostasis. The large-scale parallel locomotion tracking experiments showed a major reduction in the spontaneous activity level of the *nlrc3l* mutants and a minor reduction in the *irf8* mutants. We also analyzed the pattern of movement of each individual larva over the long-term tracking, and found no genotype-specific spatial underrepresentation, eliminating constraint motility as an explanation for the altered behavioral phenotypes. From the whole brain *in vivo* calcium imaging of the *nlr3l* mutants, we observed a decreased calcium signaling level at baseline in the diencephalic neurons compared to control siblings. RNA-Seq analysis indicated clear evidence for the presence of systemic inflammation and inappropriate activation of macrophages in the *nlrc3l* mutants consistent with previously described mutant phenotypes. In addition, we also identified a set of interesting genes that were associated with neurotransmitter transport and metabolism that were significantly down-regulated in the *nlrc3l* mutants, suggesting altered neuronal communication in these mutants that may explain for the behavioral phenotype observed.

A key difference sets apart the two microglia-lacking mutants examined in this thesis, which is that *nlrc3l* mutants have inflammatory macrophages leading to systemic inflammation (Figure 1B) whereas the *irf8* mutants have no macrophages or microglia during development because *irf8* is required for macrophage fate specification (Figure 1D) (7). Since the spontaneous behavioral deficiency is most pronounced in *nlrc3l* mutants, our data suggest that systemic inflammation may enhance the neural activity changes caused by microglia loss to induce a more severe reduction in behavioral

outcomes than in animals with only microglia loss. Taken together, our study highlights an important role for the immune system in regulating normal brain neuronal dynamics.

Methods

Details on the design and implementation of the computational analysis modules (locomotion tracking, movement pattern and calcium imaging analyses) are in the supplemental information (S1 text and Figure S1).

1. Zebrafish Large-Scale Long-term Parallel Behavior Tracking

The movements of larval zebrafish were tracked on a 96-well platform using an ultrasensitive infrared camera on a customized setup of a ZebraBox (ViewPoint Behavior Technology) over a course of 72 continuous hours i.e. 3 days. Normal 14-hour light to 10-hour dark cycles were imposed by supplying lights from 7am to 9pm each day. Experiments were conducted on genetic siblings starting from 5 dpf to 8 dpf derived from a heterozygous intercross that were individually placed in individual square housing on a 96-well format platform. Experiments were conducted blind, and genotypes were only determined after the completion of the data collection. All animals were visually inspected to be morphologically normal before placing them into the 96-well platform for behavior tracking (including features of a large inflated swim bladders, normal sized animals, and no edema). The location of every animal in the 96-well platform was recorded at an equivalent rate of 30 frames per second and values for each animal for the different metrics were integrated every 10 minutes. The outputs from ZebraBox for each experiment include a spreadsheet of raw data for all animals by variables (counts, distance, durations, etc) and the tracking images, which integrate the movement traces the animals made every 10 minutes for the entire 3-day duration of tracking.

1.1 Movement Tracking Data Mining

Large-scale raw data spreadsheets were obtained from a ZebraBox after every experiment and trimmed before analysis. Among all columns, the ones used in the downstream analysis include the following information for every individual every 10 minutes: individual location (slot) numbers (c001 – c096), start and end times of the tracked period, counts, distances and durations of non-movements, small movements and large movements. The information above for all individuals was extracted using MATLAB and converted into time plots. Additionally, the light periods were identified and separate plots and statistical analyses were generated.

1.2 Statistical Analyses for Locomotion Tracking

MATLAB scripts were generated to compute the mean and the standard errors of the means (SEM) of the counts and durations of large movements during light periods, per individual and per time point. Genotyping was performed after every experiment to identify the genotypes of the individuals. Visualizations of the statistical analysis were generated by genotype group (e.g. wild type (WT) – *nlrc3*$^{+/+}$, heterogeneous (Het) – *nlrc3*$^{st73/+}$, mutant (Mut) – *nlrc3*$^{st73/st73}$).

1.3 Analyses for Pattern of Movement

The square-shaped open field housing of each individual was divided into 3x3 squares in order to study the distribution of the individual's locations over time. Two separate scoring systems were derived to evaluate the locations near the four walls ("perimeter": squares #1,2,3,4,6,7,8 and 9) and the "center" (square #5) respectively, at each time point. The perimeter scoring system is binary and based on a cut-off value determined by user, above which the sub-square would be assigned value "1" and below which assigned value "0". The cut-off value was determined by the overall distribution of

the pixel values of all sub-squares over time to properly reduce the sensitivity of the scoring system. The scores of all 8 perimeter sub-squares were then added up together to generate the perimeter score of the individual at the time point given, ranging from 0 (no movements at all) to 8 (highly active around the walls). The scoring system for the center sub-square #5 evaluates the pixel value of each time point directly. Principal component analysis (PCA) and hierarchical clustering analysis were performed in Studio R for each set of data in order to evaluate any clustering by genotype.

2. *Whole Brain in vivo Calcium Imaging*

Nikon A1R+ confocal microscope was used for the whole brain *in vivo* Calcium imaging with GCaMP6f. The downstream analysis was performed on the imaging data from two brain regions: telencephalon and diencephalon. ImageJ was used for pre-processing including image registration and manual definition of ROIs. MATLAB scripts were generated to handle the following line of analysis: for each registered image, multiple (6~10) regions of interests (ROIs) i.e. distinct neurons were randomly selected and their calcium signaling levels for every 10 minutes were determined by the fluorescence intensity of the green fluorescent protein expression of the GCaMP6f reporter. To measure spontaneous neural activity, we determined baseline calcium signaling level (F_0) of each ROI by the average of fluorescence intensity over all time points. The detailed description of calculation of changes in calcium signaling normalized by the baseline firing, i.e. $\Delta F/F_0$ can be found under the Image Analysis Module in the supplemental information S1. Spontaneous neural activity of an ROI was determined by the counts of calcium spikes. Statistical significance for the calcium signaling level based on corrected total cell fluorescence (CTCF) and neural activity based on calcium signal changes by $\Delta F/F_0$ was determined by two-sample unpaired student's t-tests.

3. RNA-Sequencing Data Analysis

Whole animal paired-end RNA-Sequencing was performed on 10 ~ 12 pooled 4-dpf larval zebrafish by Illumina HiSeq 2x100 bp. The data processing steps were done with R packages, including quality control with *FastQC*, data trimming with *Trimmomatic*, sequencing alignment with *HISAT2*. The differential expression analysis was performed using *DESeq2* and the co-expression analysis using *EBSeq*. Detailed step-by-step instruction is available in the protocol developed by Orlando Contreras-López et al. (11). Note that the said protocol is developed for the analysis of unpaired sequencing samples; modifications of the protocol for paired-end samples were required in the steps of data trimming (12) and sequencing alignment (13).

3.1 Construction of Gene Co-Expression Network Using RNA-Seq Raw Read Counts

The co-expression networks were constructed individually for the mutants and their genetic siblings, based on the corresponding combinations of differentially expressed genes (DEGs). Such networks are undirected but weighted; the nodes are genes, and the edges are the values of the correlation between the expression levels of the two genes, between -1 and 1. 0 means the two genes do not co-express at all within this set of data. Protocol is available via Orlando Contreras-López et al. (11). The co-expression networks were visualized by the network software *Cytoscape*. Functional annotations of the DEGs were performed using the public database g:Profiler (https://biit.cs.ut.ee/gprofiler/gost).

Results

Open field long-term parallel tracking revealed reduced levels of daytime spontaneous movements of nlrc3-like mutants

Spontaneous movements of free-swimming larval zebrafish are visible and traceable by 5 dpf. In order to quantitatively characterize the spontaneous movements of the homozygous *nlrc3l* st73 mutants and *irf8* st95 mutants as well as their genetic siblings at steady state, we performed open field large-scale parallel tracking of 5-8 dpf larval zebrafish using a customized ZebraBox platform (see methods) over 72 hours (4320 minutes). Each experiment was performed double blind as genotyping was performed only afterwards. Every individual was visually inspected and checked to be morphologically normal (see methods). A consistent 14-hour light: 10-hour dark cycle was provided using. The evidence of normal active "daytime" and resting "night time" cycles is visibly apparent in all sets of animals (Figure 2B, *nlrc3l* and 2D, *irf8*).

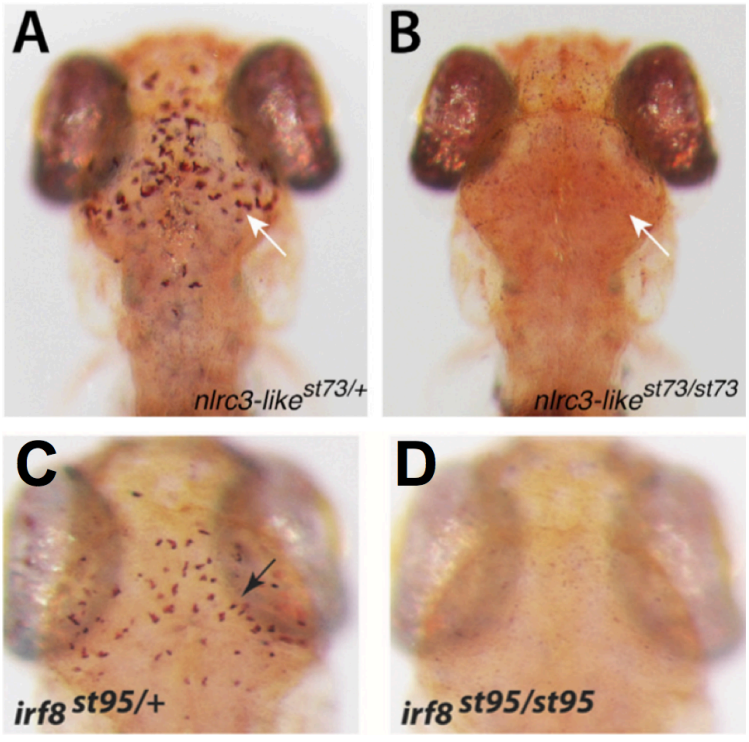

Figure 1. **Neutral-red staining of microglia in *nlrc3-like* and *irf8* mutants and control heterozygous larvae**. **A)** Normal microglia in the brain (dorsal view) of 5dpf heterozygous *nlrc3l*$^{st73/+}$ larva. **B)** No microglia in the brain of 5dpf mutant *nlrc3l*$^{st73/st73}$ larva. **C)** Normal microglia in the brain of 5dpf heterozygous *irf8*$^{st95/+}$ larva. D) No microglia in the brain of 5dpf mutant *irf8*$^{st95/st95}$ larva. Images shown in **A)** and **B)** taken from Shiau et al. 2013, and **C)** and **D)** from Shiau et al. 2015.

It was observed that the *nlrc3l* mutants (*nlrc3l*$^{st73/st73}$) had short durations (6.4 s/10min) of large, spontaneous movements comparing to their genetic siblings (*nlrc3l*$^{+/+}$: 14.9 s/10min, *nlrc3l*$^{st73/+}$: 12.1 s/10min) (Figure 2B and 2F; ****p<0.0001), but no significant difference in their average speeds (see Methods and S1; Figure 2C and 2G). A slightly weaker yet significant difference in the durations was also seen between the *irf8* mutants (*irf8*$^{st95/st95}$: 12.3 s/10min; Figure 2D and 2H; **p<0.01) and the wild-type genetic siblings (*irf8*$^{+/+}$: 15.4 s/10min), but not between the mutants and the heterozygotes (*irf8*$^{st95/+}$: 13.7 s/10min). No significant difference in the average speed was detected among the three *irf8* genotypes either (Figure 2E and 2I). Additionally, there was no significant difference in the behaviors evoked by the light/dark switches (statistical data not shown). The switch of light and dark triggered a sudden and transient increase of movements in all genotypes (Figure 1B and 1D). Therefore, a significant reduction in the levels of locomotion was detected in the *nlrc3l* mutants, as well as in the *irf8* mutants but at a more modest magnitude.

Figure 2. Microglia-lacking mutants exhibit different levels of reduction in spontaneous locomotor behavior in the daytime.

A) Schematic illustrating the experimental set-up of the large-scale zebrafish tracking on a 96-well format platform. All behaviors were tracked in mature and free-swimming larvae at the 5-8 dpf stages.

nlrc3l: (**B** and **C**), (**F** and **G**)

B) Time plot shows the locomotor movements in seconds for every 10 minute interval for the different genotypes for *nlrc3l: nlrc3l*$^{+/+}$ (black, WT), *nlrc3l*$^{st73/+}$ (gray, HET), and *nlrc3l*$^{st73/st73}$ (red, MUT) larvae. **C)** Time plot shows the speeds at which the larvae were moving over time. **F)** Box plot shows the average duration of spontaneous locomotion was significantly reduced in *nlrc3l*$^{st73/st73}$ mutants compared with control siblings. **G)** Box plot shows no significant difference in speed at which fish moved based on the three genotypes. At least 6 independent behaviors experiments were conducted representing a total number of 51 mutants among 310 fish, which all yielded the same behavioral phenotype in nlrc3l mutants.

irf8: (**D** and **E**), (**H** and **I**)

D) Time plot shows the locomotor movements in seconds for every 10 minute interval for *irf8*$^{+/+}$ (black, WT), *irf8*$^{st95/+}$ (gray, HET), and *irf8*$^{st95/st95}$ (red, MUT) larvae. **E)** Plot displays the average

speeds at which the zebrafish moved for the different *irf8* genotypes. **H)** Box plot shows the average duration of spontaneous locomotion was reduced in and *irf8*$^{st95/st95}$ mutants compared with wild type siblings. **I)** Box plot shows no significant difference in the average speed among all three genotypes. ****: p<0.0001, **: p<0.01; statistical significance was determined by a 2-tailed student's t-test.

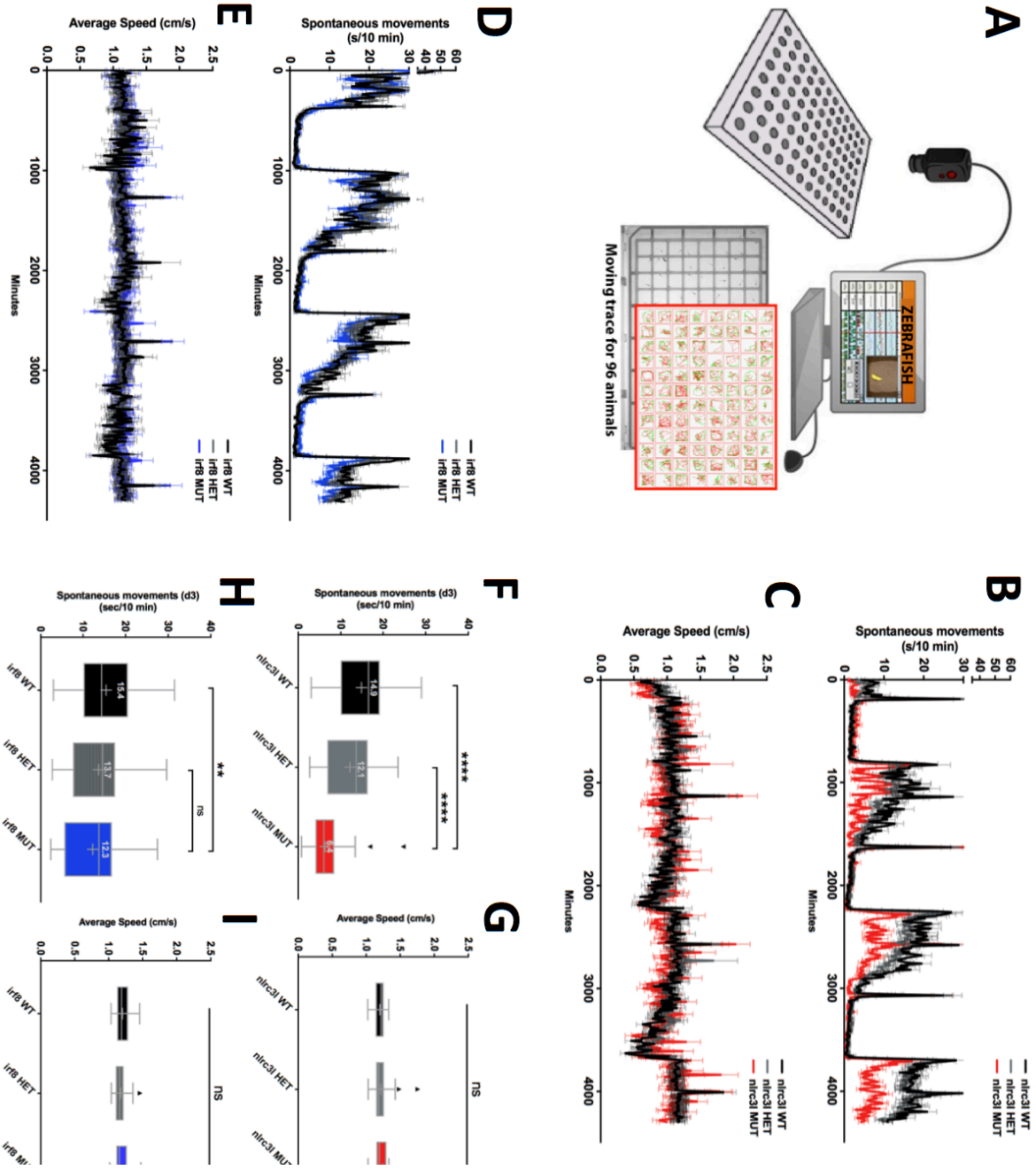

Microglia-lacking mutants did not show significantly changed pattern of movements from wild type

We next investigated whether the microglia-lacking *nlrc3l* mutants that have reduced spontaneous locomotion may also exhibit differences in their pattern of movement that may suggest increased anxiety or stress. The ultrasensitive infrared camera of the ZebraBox tracked movements on a 2-D surface and thus provided spatial information needed for the pattern analysis. In animal models such as rats and mice, in order to study the evidence for complex cognitive traits such as anxiety, a variety of environmental open field tests have been designed and analyses are designed to measure spatial variables (14). It is reported that one of such spatial measures is the exploration frequency at the center or the perimeter of an open field: the preference for perimeter, equivalent to the degree of thigmotaxis, can be used to evaluate the level of anxiety of the animal (15). We thus explored a similar idea in the larval zebrafish. By dividing the spatial locations of an individual housing cell (open field) into perimeter and center (see methods), we quantified the traces recorded of each individual larva to different locations. The goal was to examine whether there was underrepresentation of traces in the perimeter or the center specific to the mutants.

We extracted the pixel information from the images of the tracking plate taken every 10 minutes by ZebraBox for a total of 6 hours every trial (Figure 3A). Two scoring systems, one binary, the other simply based on the numerical values of pixels, were designed to evaluate the perimeter and the center behaviors of the larvae respectively (Figure 3B; see methods). We performed the scoring evaluations only for the second

---

Figure 3. **Larval zebrafish displayed similar pattern of movements based on their occupation of the perimeter for all genotypes. A)** A sample output movement traces for several individual fish over a 10 minute-interval. The green lines represent small or negligible

movements and the red lines represent large movements as defined by movement above the 0.5 cm/s speed. **B)** Every individual cell was subdivided into a 3-by-3 matrix to create the binary scoring system for the perimeter (top) and the scoring system for the center pixels (bottom). **C)** The dendrogram-heatmap and **D)** the PCA of the perimeter scores of *irf8*$^{st95/st95}$ mutants and their genetic siblings (#mut = 21, #sib = 75). **E)** The dendrogram-heatmap and **F)** the PCA of the perimeter scores of *nlrc3l*$^{st73/st73}$ mutants and their genetic siblings (#mut = 20, #sib = 76)

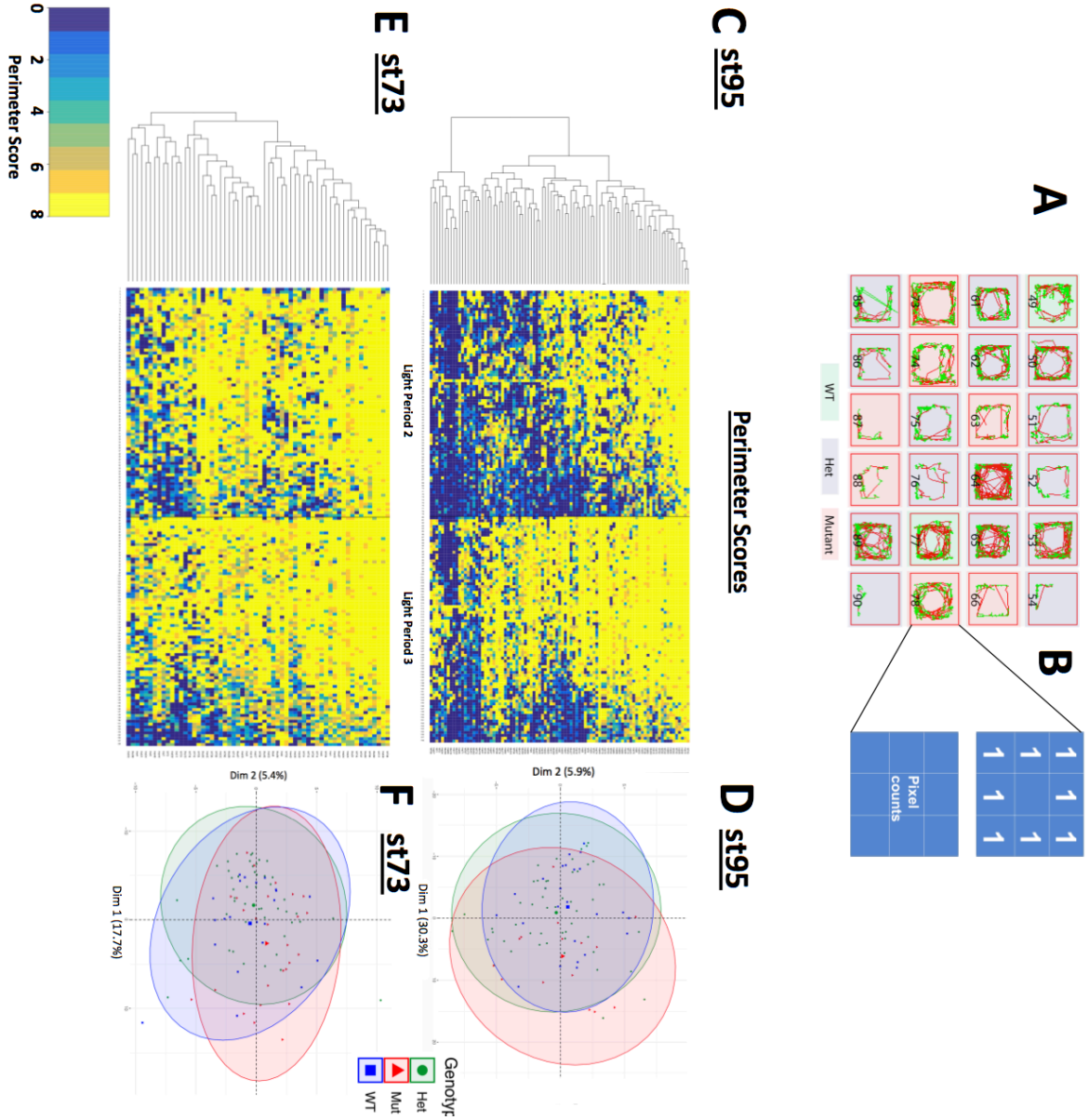

and the third light periods (daytimes of day 2 and day 3) where the activity levels were post-acclimation and expected to be more regular. Despite the highly variable patterns of movements (Figure 3A), the hierarchical clustering analysis showed no clustering of

perimeter behaviors or center behaviors by genotypes for both alleles (Figure 3C, 3E and 4A, 4C). We also confirmed by principal component analysis (PCA) that there was no genotype-specificity of spatial preferences by genotypes (Figure 3D, 3F and 4B, 4D). We were cautious to not compare the score distributions of the perimeter behaviors with those of the center behaviors, to avoid confounding the across-genotype analysis. Therefore, under the neutral, stimulus-free conditions, neither the *nlrc3l*$^{st73/st73}$ mutants nor the *irf8*$^{st95/st95}$ mutants seemed to display defected patterns of movement distinguishable from those of their genetic siblings, which also indicated that the mutants did not have constraint motility. Therefore, the negative result from the pattern of movement analysis allowed us to confirm that the mutant the phenotype was specific to a decrease in spontaneous activity.

Differential patterns of calcium spikes and waves were found in telencephalon and diencephalon in wild type, while nlrc3l mutant exhibited neural deficiency in the diencephalon region

To investigate the neural basis of the behavior phenotype in the microglia-lacking mutants, we examined whether altered neural activity in certain regions of the larval brain could explain for the reduced spontaneous locomotion using *in vivo* whole-brain calcium imaging of pan-neuronal expression of the genetically encoded calcium indicator, GCaMP6f. GCaMP6f was used to measure the changes in the cytoplasmic concentration of Ca^{2+} in the neurons. The changes in the Ca^{2+} concentration are generally in synchronization with the neuronal firing patterns.

Figure 4. **Larval zebrafish displayed similarly typical avoidance of the center region of each housing for all genotypes. A)** The dendrogram-heatmap and **B)** the PCA of the center pixels of *irf8*$^{st95/st95}$ mutants and their genetic siblings (#mut = 21, #sib = 75) showed no difference between mutants and control siblings. **C)** The dendrogram-heatmap and **D)** the PCA of the center pixels of *nlrc3l*$^{st73/st73}$ mutants and their genetic siblings (#mut = 20, #sib = 76) showed no

difference.

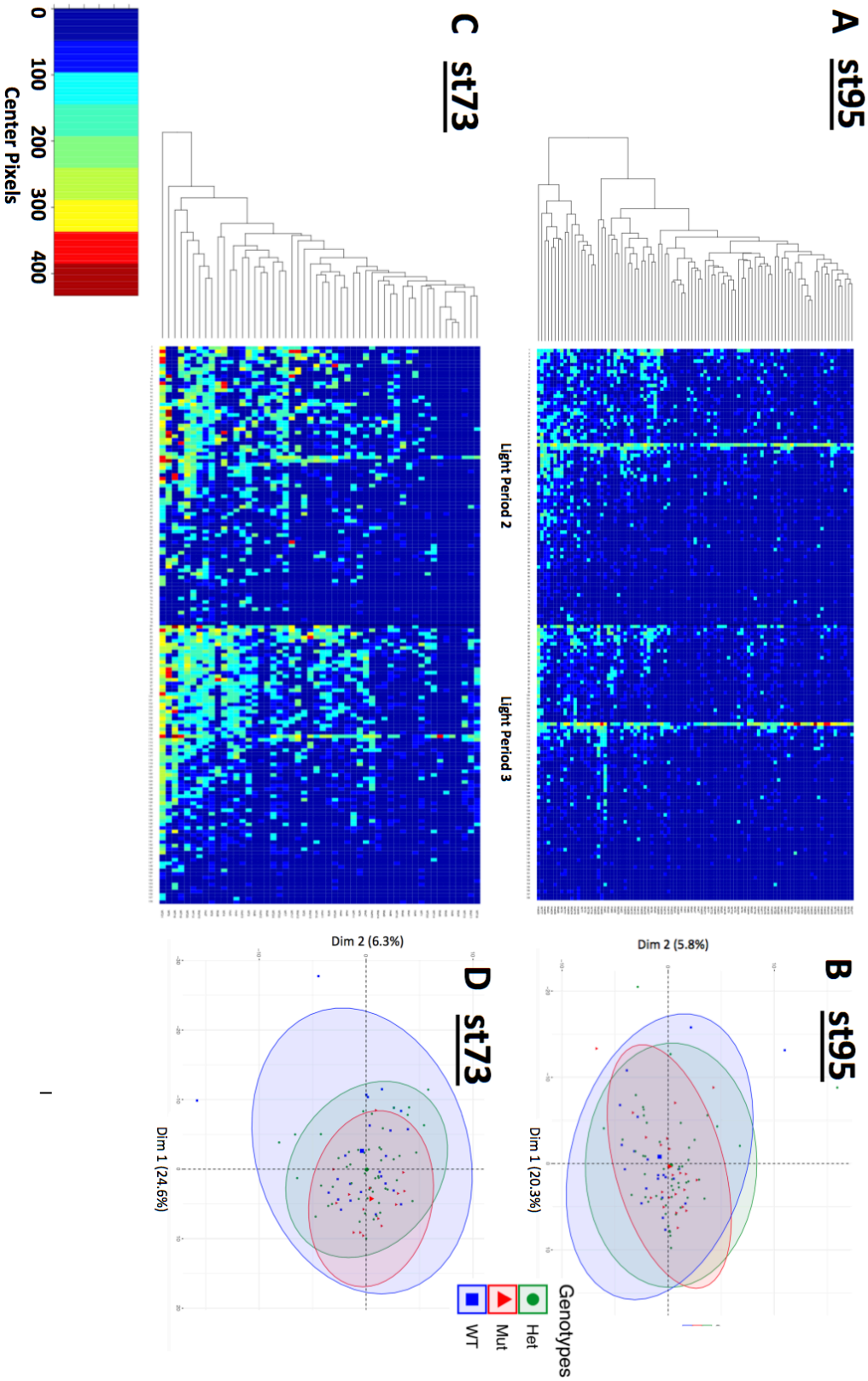
A st95
Center Pixels
B st95
C st73
D st73
Light Period 2
Light Period 3
Dim 2 (5.8%)
Dim 1 (20.3%)
Dim 2 (6.3%)
Dim 1 (24.6%)
Genotypes
WT
Mut
Het
0
100
200
300
400
Center Pixels

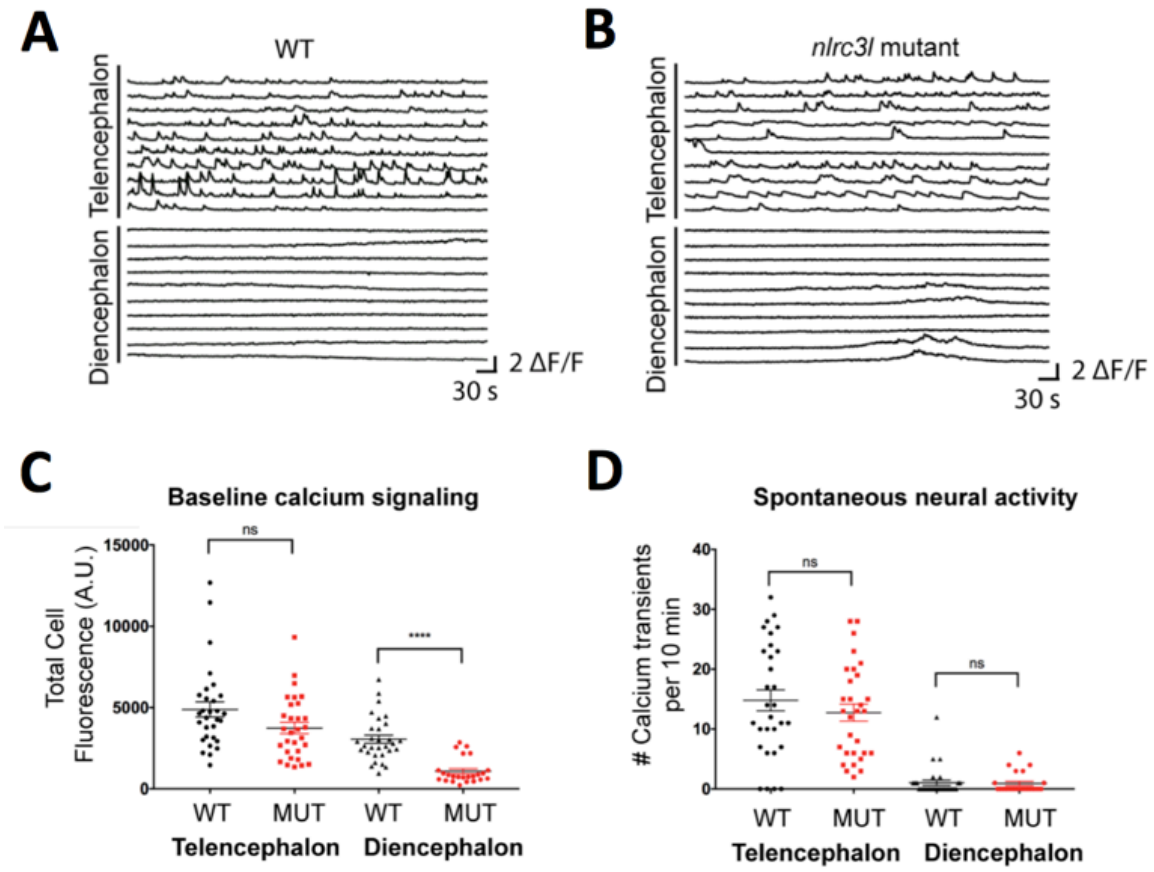

Figure 5. **Whole brain GCaMP6f *in vivo* imaging analysis of the homozygous *nlrc3l* mutants (*nlrc3l*$^{st73/st73}$) and their wild-type siblings (*nlrc3l*$^{+/+}$). A)** and **B)** display the $\Delta F/F_0$ traces for 10 individual neurons in the telencephalon (top) and another 10 neurons in the diencephalon (bottom) for a representative wild type and a representative nlrc3l mutant. **C)** Corrected total cell fluorescence (CTCF) of the calcium indicator was determined to compare baseline calcium imaging in the different brain regions for all genotypes. **D)** Spontaneous neural activity was measured based on number of calcium transients over a 10-minute imaging interval for each neuron analyzed in each brain region per genotype. ****: $p<0.0001$; statistical significance was determined by a two-sample student's t-test.

We performed the whole brain *in vivo* calcium imaging on the *nlrc3l* st73 mutants and their genetic siblings at 6 dpf after 24h of acclimation in the normal light-dark cycle. Two main brain areas of interest were the telencephalon and the diencephalon. Qualitatively, the firing patterns of the telencephalon and the diencephalon were drastically different in the wild type. The telencephalic neurons fired more frequently, as

more distinct spikes were detected within the same amount of imaging time (Figure 5A and 5B; heterozygous data not shown). However, gradual changes in the firing levels that resemble waves more than spikes with a smaller magnitude were observed in the diencephalic neurons. Quantitatively, the baseline firing levels of the diencephalic but not the telencephalic neurons of the *nlrc3l*$^{st73/st73}$ mutants were significantly lower than those of the homozygous *nlrc3l*$^{+/+}$(WT) larvae (Figure 5C). We also quantified the firing frequency i.e. the spontaneous neural activities based on the counts of calcium spikes > 0.4 ($\Delta F/F_0$), and found no significant difference between the genotypes (Figure 5D; heterozygous data not shown). The differential patterns of calcium activities found in the diencephalon of the *nlrc3l* mutants compared with wild-type siblings may explain for their reduced spontaneous locomotion.

RNA-Seq analysis indicated altered immune and neural activity in nlrc3-like mutants which can explain for the behavioral phenotype

Compared with control siblings, the *nlrc3l*$^{st73/st73}$ mutants had a larger reduction in spontaneous activity than the *irf8*$^{st95/st95}$ mutants. This may suggest that the effects of microglia loss may be exacerbated by inflammation to lead to a more severe disruption in spontaneous movements. To gain a better understanding of the molecular changes associated with the *nlrc3l* knockout, we analyzed the RNA-Seq data collected from pooled larval *nlrc3l*$^{st73/st73}$ mutants and their genetic siblings (*nlrc3l*$^{st73/st73}$ and *nlrc3l*$^{st73/+}$). In addition to the up-regulation of many inflammatory genes, we found that the changes in the expression of several neuronal function-related genes corroborate with the deficiency in neural activity in *nlrc3l* mutants based on our calcium imaging analysis.

The workflow of the RNA-Seq data analysis is illustrated schematically in Figure 6A. 358 differentially expressed genes (DEGs; $p<0.05$, >1.5 fold change) were identified, among which 245 DEGs were up-regulated and 113 down-regulated (Figure 6B and 6C).

The gene ontology (GO) annotations of all 358 DEGs showed functional differences between the two sub-groups (Figure 6D). The down-regulated DEGs were mostly associated with the oxidative-reduction process as well as metabolic processes. The up-regulated DEGs were associated with a broad range of immune response-related, even macrophage-specific GO terms, which indicate the inappropriate activation of the innate immune system that triggered systemic inflammatory responses. The enrichment of immune- and inflammation-related genes in the *nlrc3l* knockout mutants was consistent with the role of *nlrc3l* in preventing inappropriate macrophage activation and regulating inflammatory pathways ((6); unpublished data from Shiau Lab, not shown). Specifically, we identified 19 immune- or macrophage-related genes (Figure 6B), with 17/19 up-regulated and 2/19 down-regulated significantly. Among these genes are the immunoresponsive gene 1 like (*irg1l*) and aconitate decarboxylase 1 (*acod1*) which is also known as immunoresponsive gene 1 (*irg1*). While the macrophage *acod1* (*irg1*) expression in larval zebrafish was shown to respond to LPS injections (unpublished data

---

Figure 6. **RNA-Seq analysis of st73 mutants and their genetic siblings shows significant change in immune and inflammatory genes as well as a set of neural activity regulatory genes. A)** Work flow of RNA-Seq analysis. **B)** and **C)**, Volcano plots for all differentially expressed genes (DEGs) using DESeq2 . Up-regulated DEGs with $p<0.05$, red. Down-regulated DEGs with $p<0.05$, blue. Significant DEGs with Immune- and macrophage-related GO terms are labeled in **B)** and significant DEGs with neuronal transmission-related GO terms are labeled in **C)**.
D) GO annotations of the up-regulated (red) and down-regulated (blue) DEGs (above 1.5 folds change, $p<0.05$).
E) Bubble plot of the neuronal transmission-related genes and their GO terms that were significantly changed DEGs, also highlighted in **C)**.

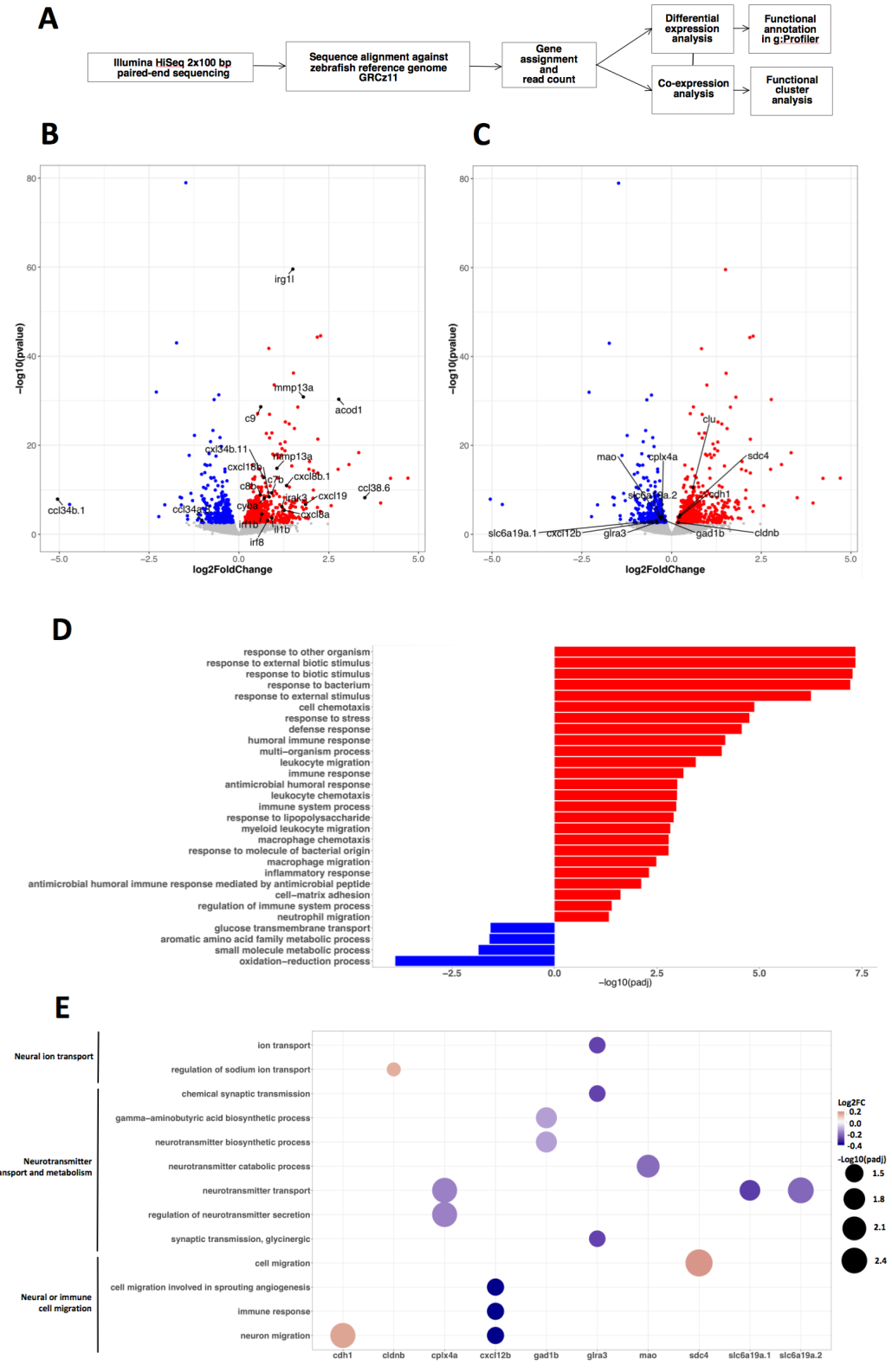
A
Illumina HiSeq 2x100 bp paired-end sequencing
Sequence alignment against zebrafish reference genome GRCz11
Gene assignment and read count
Differential expression analysis
Functional annotation in g:Profiler
Co-expression analysis
Functional cluster analysis
B
C
−log10(pvalue)
log2FoldChange
irg1l
mmp13a
acod1
c9
cxl34b.11
cxcl18b
c7b
cxcl8b.1
c8b
ccl38.6
ccl34b.1
cyba
irak3
cxcl19
ccl34a.4
cxcl8a
il1b
irf8
mao
cplx4a
clu
sdc4
slc6a19a.2
cdh1
slc6a19a.1
cxcl12b
glra3
gad1b
cldnb
D
response to other organism
response to external biotic stimulus
response to biotic stimulus
response to bacterium
response to external stimulus
cell chemotaxis
response to stress
defense response
humoral immune response
multi−organism process
leukocyte migration
immune response
antimicrobial humoral response
leukocyte chemotaxis
immune system process
response to lipopolysaccharide
myeloid leukocyte migration
macrophage chemotaxis
response to molecule of bacterial origin
macrophage migration
inflammatory response
antimicrobial humoral immune response mediated by antimicrobial peptide
cell−matrix adhesion
regulation of immune system process
neutrophil migration
glucose transmembrane transport
aromatic amino acid family metabolic process
small molecule metabolic process
oxidation−reduction process
−log10(padj)
E
Neural ion transport
Neurotransmitter transport and metabolism
Neural or immune cell migration
ion transport
regulation of sodium ion transport
chemical synaptic transmission
gamma−aminobutyric acid biosynthetic process
neurotransmitter biosynthetic process
neurotransmitter catabolic process
neurotransmitter transport
regulation of neurotransmitter secretion
synaptic transmission, glycinergic
cell migration
cell migration involved in sprouting angiogenesis
immune response
neuron migration
cdh1
cldnb
cplx4a
cxcl12b
gad1b
glra3
mao
sdc4
slc6a19a.1
slc6a19a.2
Log2FC
-Log10(padj)

from Shiau Lab, not shown), the early expression of *irg1l*, the homolog of human and murine immunoresponsive gene 1 is found in the epithelial cells in zebrafish; both are reported to be highly up-regulated after bacterial exposure (16). A pro-inflammatory marker, interleukin 1 beta (*il1b*) was also found significantly up-regulated but with a lower fold change. We also identified 11 DEGs associated with neural ion transport, neurotransmitter transport and metabolism and neural or immune cell migration, 4/11 up-regulated and 7/11 down-regulated. In particular, gene *clu* (clusterin) is the most up-regulated DEG among the four and it is known to protect against protein aggregation and neuronal death**.** Interestingly, as revealed by their GO annotations, all 7/7 down-regulated genes were associated with neurotransmitter transport and metabolism (Figure 6E). This provides the impaired neurotransmitter activities as a potential explanation for the decreased baseline firing level of the diencephalic neurons in the *nlrc3l* mutants (Figure 5C).

Unexpectedly, multiple members of the structural protein crystallin family showed up in the largest and most highly connected components of the co-expression networks (Figure 7A and 7B). The expressions of these crystallin genes were found in the lens at the various developmental stages of zebrafish the earliest (17). However, the qPCR analysis (unpublished data from Shiau Lab, not shown) was not consistent with the inference from the co-expression analysis. The dendrogram-heatmap on the larger co-expression network ($p<0.05$; Figure 7C) showed some subtle clustering of co-expression levels: the largest two blocks (upper right corner of Figure 7C) were dominated by the crystallin family. Further functional analysis of different parts of the co-expression networks showed no functional modules in addition to the GO analysis of the DEGs

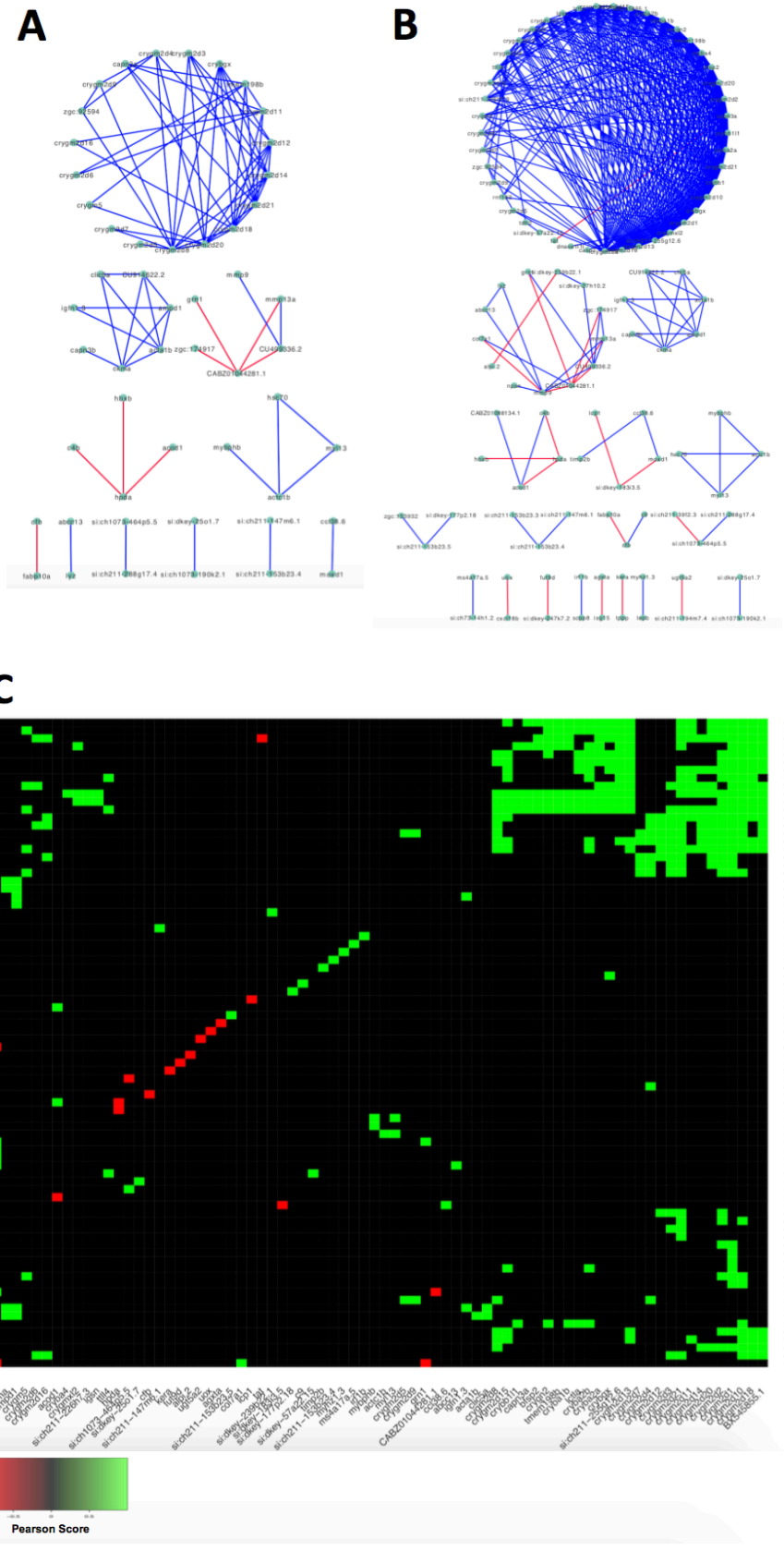
A
B
C
Pearson Score

Figure 7. Co-expression analysis of the RNA-seq data set for nlrc3l mutants compared with control siblings. A) The network visualizations of gene co-expressions with p<0.01. **B)** The network visualizations of gene co-expressions with p<0.05. **C)** The dendrogram-heatmap of the co-expression pairs in **B)** (p<0.05).

---

above and thus did not provide more information (data not shown). It was then suspected that many genes in the networks were markers instead of functionally related genes. The RNA-Seq analysis provided evidence of up-regulation of systemic immune response and macrophage over-activation as well as down-regulation of neurotransmitter activities such as transportation and metabolism in the larval *nlrc3l*$^{st73/st73}$ mutants.

Discussion

The goal of this study was to investigate the possible role of microglia in the modulation of brain neural activity that govern animal behavior. Because microglia are critical for maintaining the normal healthy brain at homeostasis, we tested whether microglia may ultimately affect spontaneous, steady state behavior of larval zebrafish in a neutral, stimulus-free environment. It remains elusive whether the brain immune cells can significantly shape the function of the brain. We hypothesized that microglia are intricately interconnected with neuronal activity and thus neural circuit function, thereby may be able to alter behavioral outputs of brain functions.

The study was conducted on the two previously generated stable mutant lines that have no microglia, with loss-of-function (LOF) mutations in the genes *nlrc3-like* and *irf8* respectively. The st73 LOF mutation in *nlrc3-like* gene causes inappropriate activation of primitive macrophages, which consequently fail to differentiate into microglia in brain while triggering systemic inflammation in zebrafish. On the other hand, the other microglia-lacking mutant has a loss of microglia for an entirely different reason. The homozygous *irf8* st95 mutants are unable to form microglia because of the loss of

primitive macrophages at an early stage. We performed parallel experiments and analyses on these two mutant lines in larvae to allow us to use two independent mutant lines to test the role of microglia on brain function and behavior.

We found that the homozygous *nlrc3l* st73 mutants exhibited highly significantly reduced levels of movements comparing to their genetic siblings, while a more modest but still significant decrease was also observed in the homozygous *irf8* st95 mutants comparing to their genetic siblings. And second, there was no genotype-specific spatial preference (the perimeter versus the center of the open field) of the mutants in comparison with those of their genetic siblings. We also performed whole brain *in vivo* GCaMP6f imaging and RNA-Seq analysis on the homozygous *nlrc3l* st73 mutant larvae as compared with their wild type and heterozygous genetic siblings. Significantly lower baseline neuronal firings were detected in the diencephalon but not the telencephalon of the mutants. The RNA-Seq data exhibited transcriptomics evidence that supported the phenotypes observed in the homozygous *nlrc3l* st73 mutants. On the other hand, the co-expressions revealed several potential candidate genes for future studies: the expression level of *hpda* (4-hydroxyphenylpyruvate dioxygenase a) was negatively correlated with that of *acod1* (*irg1*); *cfb* (complement factor B) was negatively correlated with *fabp10a* (fatty acid binding protein 10a); *irf1b* (interferon regulatory factor 1b) was positively correlated with *scpp8* (secretory calcium-binding phosphoprotein 8). Given all evidence above, we concluded that microglia loss, potentially also inflammation, is sufficient to disturb the neural circuit of spontaneous movements in larval zebrafish.

However, further studies are required to confirm the effects of inflammation on the neural circuits of spontaneous movements. From the movement tracking analysis, we report the differentially reduced levels of movements in the homozygous *nlrc3l* st73 mutants and *irf8* st95 mutants in comparisons with their genetic siblings respectively. Since the GCaMP6f imaging was only performed on the homozygous *nlrc3l* st73

mutants and their genetic siblings, the region-specific firing patterns in the brain of the homozygous *irf8* st95 mutants and their genetic siblings are still unknown. In order to confirm the low baseline firing in the diencephalon of the homozygous *nlrc3l* st73 mutants are strictly attributed to the negative impact of inflammation-specific mechanism in addition to impaired microglia, we expect to see normal baseline firings in the diencephalon of the homozygous *irf8* st95 mutants. If decreased or increased baseline firings were observed, more follow-up experiments would be required to identify the exact mechanism behind. One potential experiment would be to overexpress global cytokines such as TNFα and IL-1β into the genetic siblings of the homozygous *irf8* st95 mutants to introduce inflammation. In the future, we would also perform RNA-Seq on the homozygous *irf8* st95 mutants and their genetic siblings to identify differentially expressed genes (DEGs) and functional modules. The *nlrc3l* st73 RNA-Seq analysis presented in this thesis was performed on whole animals; in order to detect shifts in expression profiles in the neuroimmune system of the mutants at a higher resolution, an improved RNA-Seq analysis for both the *nlrc3l* st73 and the *irf8* st95 mutant lines should be brain region-specific. Directed by the findings from the calcium imaging analysis, one of the brain regions of interest would be the diencephalon. Future studies should also be conducted to pinpoint the sub-populations of the neurons in diencephalon with decreased neuronal firings in the homozygous *nlrc3l* st73 mutants, and to map out the neural circuit for spontaneous movements. Further experiments are needed to identify the roles of the sub-regions of diencephalon in the spontaneous movements of larval zebrafish. We were able to conclude with confidence that microglia are required to mediate the normal neural activity associated with spontaneous movements in larval zebrafish, but future studies are needed to confirm whether systemic inflammation can modulate these neural activities.

Interestingly, the RNA-Seq analysis also revealed a set of significantly down-regulated DEGs associated with neurotransmitter transport and metabolism. However, the identities of cell type affected remain unclear. It is possible the down-regulation of such neurotransmitter gene expressions is due to the lack of the microglial population, which is also able to express receptors for neurotransmitters such as GABA, glutamate and dopamine (8). Alternatively, if the down-regulations were specific to a certain neuronal sub-population, it is possibly a result of the lack of interconnection between microglia and neurons. In order to understand the mechanism behind the microglial regulation of neuronal functions, future studies should investigate the types of neurotransmitter and the cell types affected.

In summary, insights from our investigations in zebrafish will likely be relevant to human mechanisms as many brain and microglial processes are conserved and that 70% of known genes affecting human diseases have functional orthologs in zebrafish. Our study highlights an important role for the immune system in regulating normal brain neuronal dynamics.

Contributions

Peiwen Cai (P.C.) and Celia E. Shiau (C.E.S) developed the computational pipelines for analyzing the large datasets of zebrafish behavior and calcium brain imaging. P.C. wrote all the MATLAB and R scripts for the study, and conducted the analysis of the RNA-Seq data and locomotion patterns. Cameron Dixon performed all the behavior experiments, *in vivo* brain imaging, and genotyping. C.E.S designed and supervised the project as well as performed data analysis using the computational pipelines.

ACKNOWLEDGEMENTS

This work was supported by the UNC Provost Junior Faculty Development Award, Startup Funds, and NIH MIRA grant to the principal investigator and my thesis mentor Celia E. Shiau. I would like to thank my mentor Celia E. Shiau for the long-term mentorship and supports during my time as an undergraduate student in the Shiau Lab, and Cameron Dixon for conducting the experiments. I also thank the past and current members of the Shiau Lab and highlight a special thanks to Mark Kate Christiansen who is a future medical doctor full of potential.

References

1. Cui C, Spaink HP, Stockhammer OW, Zakrzewska A, Meijer AH, Benard EL. Macrophage-specific gene functions in Spi1-directed innate immunity. Blood. 2010;116(3):e1–11.
2. Van Ham TJ, Kokel D, Peterson RT. Apoptotic cells are cleared by directional migration and elmo1-dependent macrophage engulfment. Curr Biol [Internet]. 2012;22(9):830–6. Available from: http://dx.doi.org/10.1016/j.cub.2012.03.027
3. Kalicharan RD, Brady CA, Sjollema KA, Giepmans BNG, Peterson RT, Kuipers J, et al. Intravital correlated microscopy reveals differential macrophage and microglial dynamics during resolution of neuroinflammation. Dis Model Mech. 2014;7(7):857–69.
4. Becker TS, Rinkwitz S, Lieschke GJ, Svahn AJ, Graeber MB, Bennett MR, et al. Development of ramified microglia from early macrophages in the zebrafish optic tectum. Dev Neurobiol. 2012;73(1):60–71.
5. Meireles AM, Shiau CE, Guenther CA, Sidik H, Kingsley DM, Talbot WS. The phosphate exporter xpr1b is required for differentiation of tissue-resident macrophages. Cell Rep [Internet]. 2014;8(6):1659–67. Available from:

http://dx.doi.org/10.1016/j.celrep.2014.08.018

6. Shiau CE, Monk KR, Joo W, Talbot WS. An anti-inflammatory nod-like receptor is required for microglia development. Cell Rep [Internet]. 2013;5(5):1342–52. Available from: http://dx.doi.org/10.1016/j.celrep.2013.11.004
7. Shiau CE, Kaufman Z, Meireles AM, Talbot WS. Differential requirement for irf8 in formation of embryonic and adult macrophages in zebrafish. PLoS One. 2015;10(1):1–15.
8. Pocock JM, Kettenmann H. Neurotransmitter receptors on microglia. Stroke Vasc Neurol. 2016;1(2):52–8.
9. Kettenmann H, Kirchhoff F, Verkhratsky A. Microglia: New Roles for the Synaptic Stripper. Neuron [Internet]. 2013;77(1):10–8. Available from: http://dx.doi.org/10.1016/j.neuron.2012.12.023
10. Li Y, Du XF, Liu CS, Wen ZL, Du JL. Reciprocal Regulation between Resting Microglial Dynamics and Neuronal Activity In Vivo. Dev Cell [Internet]. 2012;23(6):1189–202. Available from: http://dx.doi.org/10.1016/j.devcel.2012.10.027
11. Ristova D. Root Development: Methods and Protocols [Internet]. Vol. 1761. 2018. Available from: http://link.springer.com/10.1007/978-1-4939-7747-5
12. Bolger AM, Lohse M, Usadel B. Trimmomatic: A flexible trimmer for Illumina sequence data. Bioinformatics. 2014;30(15):2114–20.
13. Kim D, Langmead B, Salzberg SL. HHS Public Access. Nat Methods. 2016;12(4):357–60.
14. Archer J. Tests for emotionality in rats and mice: A review. Anim Behav. 1973;21(2):205–35.
15. Simon P, Dupuis R, Costentin J. BEHAVIOURAL BRAIN RESEARCH Thigmotaxis as an index of anxiety in mice. Influence of dopaminergic

transmissions. Bchavioural Brain Rcsearch [Internet]. 1094;61(1094):59–64. Available from: http://ac.els-cdn.com/0166432894900086/1-s2.0-0166432894900086-main.pdf?_tid=8ca468a8-5165-11e7-91e6-00000aacb35d&acdnat=1497488405_2fd7bcb865141af64eac339a5d4067bf

16. Van Soest JJ, Stockhammer OW, Ordas A, Bloemberg G V., Spaink HP, Meijer AH. Comparison of static immersion and intravenous injection systems for exposure of zebrafish embryos to the natural pathogen Edwardsiella tarda. BMC Immunol. 2011;12.

17. Greiling TMS, Houck SA, Clark JI. The zebrafish lens proteome during development and aging. Mol Vis [Internet]. 2009;15(July):2313–25. Available from: http://www.pubmedcentral.nih.gov/articlerender.fcgi?artid=2779061&tool=pmcentrez&rendertype=abstract